A Model for Shelled Micro-bubble in Geometric Confinement Under Acoustics Field

Adnan Qamar

Division of Physical Sciences and Engineering, King Abdullah University of Science and Technology (KAUST), Thuwal 23955, KSA

† *Corresponding Author Email*: *Adnan.Qamar@kaust.edu.sa*

(Received ——; accepted ——)

ABSTRACT

A theoretical model to predict the dynamics of a shelled micro-bubble driven by acoustic field in a tubular geometric confinement is proposed in the present study. The model is derived from first principle and may not be considered as a variant of Rayleigh-Plesset solution. A semi-analytical model is derived in the form of an ordinary differential equation connecting all parameters involved. Results obtained are in agreement with the available experimental data. The model is further linearized to obtain expression for the forced resonant frequency, which is shown to depend on geometric parameter of confinement as $D/\sqrt{L}$ where D and L are the tube diameter and length, respectively. Further, linear viscous damping coefficient is also studied and is found that an overdamped or an underdamped state exist base on shelled micro-bubble size and parameters of geometric confinement (L and D). The state of damping clearly indicate when the shelled micro-bubble in confinement would respond linearly or non-linearly under the influence of acoustic field.

Keywords: Shelled micro-bubbles, acoustics, geometric confinement, bubble dynamics, bubble resonant frequency, ultrasound contrast agents.

NOMENCLATURE

R_1	internal radius of the UCA	V_r	radial fluid velocity
R_2	external radius of the UCA	V_z	axial fluid velocity
L	half length of the tube	V_{CL}	tube center-line fluid velocity
ρ_F, ρ_S	density of the fluid and shell, respectively	$\bar{U}$	fluid average velocity
μ_F, μ_S	viscosity of the fluid and shell, respectively	D	diameter of the tube
P_G	bubble pressure	f_r	resonant frequency
P_a	atmospheric pressure	t	time
σ_1, σ_2	surface tension at internal and external interface		

1. INTRODUCTION

Shelled micro-bubbles have been conventionally used as Ultrasound contrast agents (UCAs) to improve the quality of acquired medical images. Typically, these UCAs are gas micro-bubbles in the size range of $0.5 - 10\mu m$, and are encapsulated by a thin shell of albumin, polymer, or lipid (Doinikov and Bouakaz 2011). This thin shell structure around the shelled micro-bubbles aids in stabilizing against fast dissolution and coalescence. The shelled micro-bubbles have a higher compressibility compared to the surrounding fluid/tissue. As such, they act as high ultrasound scattering particles.

The dynamical response (linear or non-linear) and resonant properties of these shelled micro-bubbles or UCAs are utilized to enhance the contrast of the acquired medical images, thereby, leading to better diagnostics. Recent uses of shelled micro-bubbles include several areas of applied research such as targeted drug and genes delivery (Dayton and Ferrara 2002; Klibanov 2006), thrombus dissolution (Unger, Matsunaga, McCreery, Schumann, Sweitzer, and Quigley 2002), gas embolotherapy (Qamar, Wong, Fowlkes, and Bull 2012; Z.Z.Wong, Kripfgans, Qamar, Fowlkes, and Bull 2011), sonoporation (Cosgrove and Harvey 2009) and micro-pumping (Ryu, Chung, and Cho 2010). These newly emerging application areas would benefit from a better understanding and modeling of the dynamics of these shelled micro-bubbles, especially in small confined spaces such as blood vessels and channels of various sizes.

Over the last several decades, extensive studies and mathematical models have been proposed to predict and elucidate the dynamics of unconfined shell micro-bubbles (surrounded by an infinite pool of fluid). The basis of all existing math-

ematical models is the Rayleigh-Plesset solution for the free bubble (unconfined and no-shell assumed). There also exists, a vast amount of literature on unconfined shelled micro-bubbles. A comprehensive review of these models and studies is presented in Refs. (Leighton 1994; Doinikov and Bouakaz 2011). However, modeling of constrained shelled micro-bubbles or UCAs is fairly limited and not much is known about the dynamics of these shelled micro-bubbles under confined spaces while driven by acoustic field. Experimental studies (F.Caskey, Kruse, Dayton, Kitano, and W.Ferrara 2006; Sassaroli and Hynynen 2004; Sassaroli and Hynynen 2006; P.Zhong, Zhou, and Zhu 2001; Zheng, Dayton, Caskey, Zhao, Qin, and Ferrara 2007; Caskey, Kruse, Dayton, and Ferrara 2005; Garbin, D.Cojoc, E.Ferrari, Fabrizio, Overvelde, Meer, Jong, D.Lohse, and Versluis 2007) have shown that there is a significant alteration in dynamic response, when shelled micro-bubbles are sonicated in confined spaces such as small phantom vessels or channels. Few semi-analytical mathematical models (Atkisson 2008) have been proposed for bubble sonication inside a confined space under idealistic, limiting assumptions (Atkisson 2008). Owing to the challenges associated with these models and their limiting assumptions, direct numerical computations (Qamar, Wong, Fowlkes, and Bull 2012; Ye and Bull 2004) have also been carried to investigate bubble (no-shell) expansion in small tubes undergoing sonication. These full scale numerical computations have provided useful insights into the various phenomena (particularly on evolving flow field) associated with micro-bubble sonication in confined spaces.

The proposed model is derived by assuming a rigid tube wall, which physiologically can represents any arterial or ventricle vessel which can be assumed as structurally rigid. For small blood vessels, like capillaries, the flexibility of the wall is essential to consider. Under such scenario, the bubble generally has an lateral elongated shape during expansion phase. The emerging flow field inside the compliant vessel (or tube) needs to be solved to determine the pressure distribution. The pressure distribution inside the flexible tube will be different in radial and streamwise directions and can only be determined by full numerical solution of the compressible Navier-Stokes (Qamar, Hasan, and Sanghi 2010; Qamar, Hasan, and Sanghi 2006). Besides, for bubble the radial momentum equation is not applicable, and therefore a generalized form of the compressible equation using the interface tracking method (Gueyffier, Li, Nadim, Scardovelli, and Zaleski 1999)will be required. On the other side, the compliance of a blood vessel and its mechanical response to evolving stresses are complex to model as blood vessels behave in a non-linear fashion themselves (Humphrey and Na 2002; Misra and Singh 1983). Given these challenges, the flexible wall model is challenging to implement in symmetric models of UCAs.

In the present study, a theoretical semi-analytical model is derived for the shelled micro-bubble in geometric confinement while undergoing sonication. The model is not based on the Rayleigh-Plesset solution. In fact, it may be viewed as a first principle derivation from the reduced Navier-Stokes equation. The primary objective of this work is to propose a model of the dynamics of an shelled micro-bubble or UCA in a tubular geometry with circular cross-section. Furthermore the guiding principle of the analysis is to provide practitioners in this field with applicable formula for quantities such as resonant frequency and its influence on geometric confinement parameters. The choice of a circular cross-section stems from our interest in modeling the UCA dynamics in an blood vessel and this model can be easily extended/modified for other cross-sections by straight-forward adjustments to the derivation.

2. Theoretical Formulation

A schematic diagram in Fig. 1, depicts the physical setup for the model derivation, along with the respective physical properties of the three components, G (gas bubble), S (shell), and F (surrounding liquid). A single shelled micro-bubble or UCA with an inital internal radius of $(R_1)_0$ and an outer radius of $(R_2)_o$ (with shell thickness of $\delta = (R_2)_o - (R_1)_o$) is located at the center of the circular cross-section tube of diameter (D) and length (L). The tube is open at both ends with a known pressure P_L. It is assumed that the bubble remains spherical throughout the acoustic radiation. This assumption is consistent with the experimental observations for confined UCAs (Zheng, Dayton, Caskey, Zhao, Qin, and Ferrara 2007). Further, the shell material is assumed to behave like Newtonian viscous fluid as utilized in some previous studies for unconfined micro-bubbles (Doinikov and Bouakaz 2011).

Apply Mass conservation around the bubble surface yields,

$$4\pi R_2^2 \frac{dR_2}{dt}\rho_s = 4\pi r^2 V_r \rho_s \tag{1}$$

where, V_r is the fluid velocity in radial direction and ρ_s is the density of the shell material. Therefore, the fluid radial velocity is given by,

$$V_r = \frac{R_2^2}{r^2}\frac{dR_2}{dt} \tag{2}$$

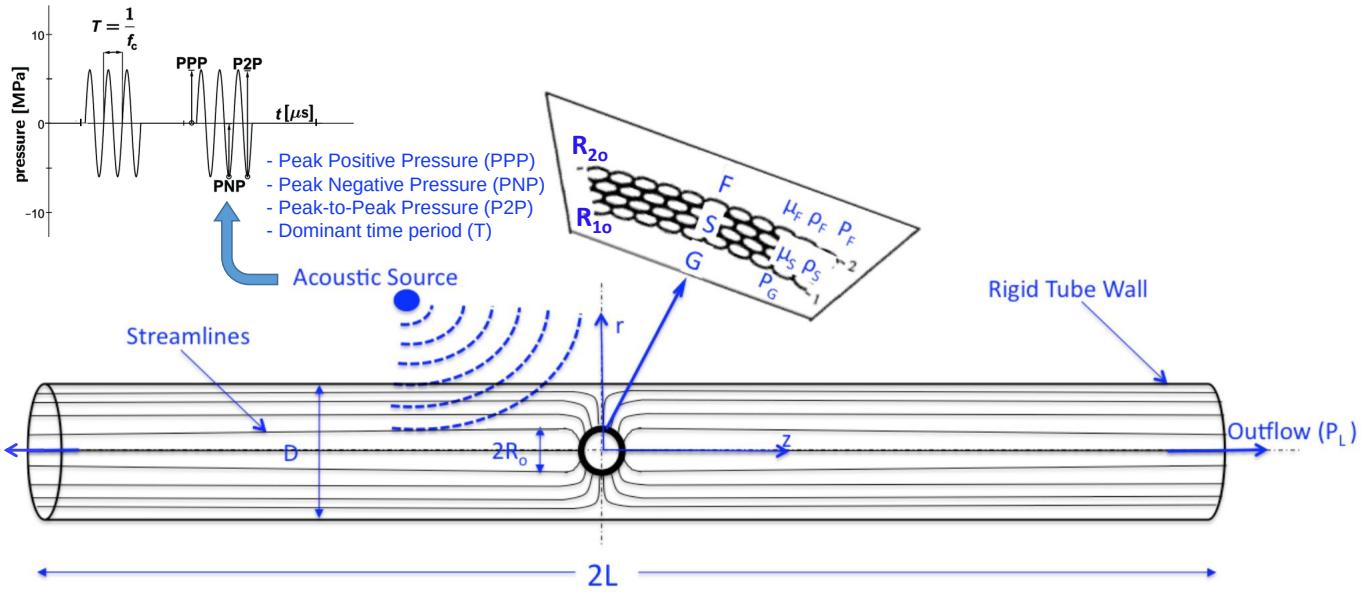

Fig. 1. Schematic of the shelled micro-bubble in geometric confinement with typical acoustic pulse used in UCA sonication.

The radial momentum equation is given by :

$$\rho_s\left(\frac{\partial V_r}{\partial t}+V_r\frac{\partial V_r}{\partial r}\right)=-\frac{\partial p}{\partial r}+\frac{1}{r^2}\frac{\partial(r^2\,T^s_{rr})}{\partial r}+\frac{T^s_{rr}}{r} \tag{3}$$

where, T^s_{rr} represent the normal stress in radial direction of shell material. Integrating above momentum equation from R_1 to R_2 yields,

$$\rho_s\int_{R_1}^{R_2}\left(\frac{\partial V_r}{\partial t}+V_r\frac{\partial V_r}{\partial r}\right)dr=\int_{R_1}^{R_2}\left(-\frac{\partial p}{\partial r}+\frac{1}{r^2}\frac{\partial(r^2\,T^s_{rr})}{\partial r}+\frac{T^s_{rr}}{r}\right)dr \tag{4}$$

$$\rho_s\left[\frac{R_1(R_2-R_1)}{R_2}\frac{d^2R_1}{dt^2}+\left(\frac{dR_1}{dt}\right)^2\left(\frac{3}{2}+\frac{R_1^3-4R_2^3}{2R_2^3}\left(\frac{R_1}{R_2}\right)\right)\right]=P_G(t)+T^L_{rr}(R_2,t)-\frac{2\sigma_1}{R_1}-\frac{2\sigma_2}{R_2}-P_L(R_2,t)+\int_{R_1}^{R_2}\frac{3T^s_{rr}}{r}dr \tag{5}$$

where, σ_1 and σ_2 represents the surface tension at R_1 and R_2 interfaces, while P_G, P_s and P_L represents gas, shell and liquid pressure, respectively. The normal jump conditions at both interfaces R_1 and R_2 are utilized for pressure gradient term, given by:

$$P_G(t)=P_s(R_1,t)-T^s_{rr}(R_1,t)+\frac{2\sigma_1}{R_1}\quad at\quad r=R_1$$

$$P_s(R_2,t)-T^s_{rr}(R_2,t)=P_L(R_2,t)-T^L_{rr}(R_2,t)+\frac{2\sigma_2}{R_2}\quad at\quad r=R_2 \tag{6}$$

In eq.(5), as discussed above the shell material is assumed to behaves as Newtonian fluid, thus the integral term can be represented as,

$$T^s_{rr}=2\mu_s\frac{\partial V_r}{\partial r} \tag{7}$$

$$T^s_{rr}=-4\mu_s\frac{R_1^2}{r^3}\frac{dR_1}{dt} \tag{8}$$

$$\int_{R_1}^{R_2}\frac{3T^s_{rr}}{r}dr=4\mu_sR_1^2\frac{dR_1}{dt}\left[\frac{1}{R_2^3}-\frac{1}{R_1^3}\right] \tag{9}$$

It is to be noted here that the any shell material (such as, pseudoplastic, dilatant, plastic or viscoelastic fluids) with known constitutive relationship can be utilized (Doinikov and Bouakaz 2011). Here, for simplicity, the shell is assumed to behave like viscous Newtonian fluid. Therefore, under Newtonian fluid assumption the final form of momentum equation governing the shell is given

by:

$$\rho_s\left[\frac{R_1(R_2-R_1)}{R_2}\frac{d^2R_1}{dt^2}+\left(\frac{dR_1}{dt}\right)^2\left(\frac{3}{2}+\frac{R_1^3-4R_2^3}{2R_2^3}\left(\frac{R_1}{R_2}\right)\right)\right]+4\mu_F\frac{R_1^2}{R_2^3}\frac{dR_1}{dt}+\frac{2\sigma_1}{R_1}+\frac{2\sigma_2}{R_2}-4\mu_s R_1^2\frac{dR_1}{dt}\left[\frac{1}{R_2^3}-\frac{1}{R_1^3}\right]=P_G(t)-P_L(R_2,t) \quad (10)$$

The bubble pressure $P_G(t)$ is assumed to follow Polytropic Ideal gas law given by,

$$P_G(t)=P_o\left(\frac{R_o}{R_1}\right)^{3\gamma}+P_a \quad (11)$$

where P_o is the initial bubble pressuer, P_a is the externally applied acoustic pressure, γ is the polytropic coefficient ($\gamma=1$ for isothermal process and $\gamma=1.4$ for adiabatic process). For UCAs, nitrogen or perfluorocarbon gas cores are used in most medical applications (Lindner 2004) with γ values in range of 1-1.6. The only unknown in eq.(11) is $P_L(R_2,t)$ which can be determined from the evolving fluid flow inside the circular tube. This can be achieved by integrating momentum equation along the center-line of the circular tube from R_2 to L.

If the tube diameter is small, the symmetric bubble motion is greatly influenced during sonication, and it has a tendency to deviate from the spherical shape. From a mathematical perspective, no relationship exists to quantify D and Ro, when the symmetric bubble nature is compromised. However, for a simple gas bubble in a tube, Oguz and Prosperetti (Oguz and Prosperetti 1998) demonstrated that a bubble of approximately 2-3 times smaller than the tube could maintain a spherical symmetry. This was demonstrated by comparing the symmetric model with respect to the boundary integral method. Similar findings are observed in Caskey et al. (F.Caskey, Kruse, Dayton, Kitano, and W.Ferrara 2006) experimental work. Narrow tubes in the range of 12-195 m were used to insonicate micro-bubble between 1-5 m size, and mostly symmetric nature was observed during the high-speed imaging. The proposed simplified model relies on this symmetric assumption framework and is only useful for scenarios where it is evident that the bubble remains spherical during acoustic perturbation.

During sonication, if the bubble remain spherical during the growth and collapse, then the flow induce by bubble motion is symmetric (Qamar, Samtaney, and Bull 2013; Doinikov and Bouakaz 2011). Therefore, following assumptions are reasonable valid:
(a) Away from bubble, radial and swirl components of velocities are zero (i.e, $V_r=V_\theta=0$)
(b) The flow is axisymmetric (i.e, $\partial/\partial\theta=0$)
(c) Radial momentum diffusion is much greater than the axial momentum diffusion, therefore, axial momentum diffusion can be neglected (i.e, $\partial^2V_z/\partial z^2\approx 0$)

Under the light of these valid assumptions, the axial momentum equation can be simplified as :

$$\rho_F\frac{\partial V_z}{\partial t}=-\frac{\partial p}{\partial z}+\mu_F\left[\frac{1}{r}\frac{\partial}{\partial r}\left(r\frac{\partial V_z}{\partial r}\right)\right] \quad (12)$$

It is to be noted that above equation is similar to Poiseuille flow axial momentum equation (Pritchard 2011). Therefore, a general solution for axial velocity component can be given by,

$$V_z=V_{CL}\left[1-(\eta-1)\left(\frac{2r}{D}\right)^2\right] \quad (13)$$

where, V_{CL} represent the tube centerline velocity and r is the radial coordinate. The constant η decide the shape of the boundary layer profile evolving within the tube by bubble oscillation due to sonication. If $\eta=2$ is used, it will results in a parabolic profile, whereas $\eta=1$ will result in a plug flow profile ($2>\eta>1$).

Using above generalized velocity profile the flow rate through the tube is given by:

$$Q=\int_0^{D/2}2\pi rV_z dr=\int_0^{D/2}2\pi rV_{CL}\left[1-(\eta-1)\left(\frac{2r}{D}\right)^2\right]dr=V_{CL}\frac{(3-\eta)}{2}\frac{\pi D^2}{4} \quad (14)$$

Now the average velocity can be computed using:

$$\bar{U}=\frac{Q}{A}=\frac{(3-\eta)}{2}V_{CL} \quad (15)$$

The tube centerline velocity in terms of average tube velocity is then given by,

$$V_{CL}=\alpha\bar{U} \quad where, \quad \alpha=\frac{(3-\eta)}{2} \quad (16)$$

The average velocity and in turn the centerline velocity is primarily dependent on shelled microbubble response under acoustic field. To obtain induced average velocity in the tube, mass conservation is applied to the entire tube length which yields:

$$\frac{d}{dt}\left[\frac{L\pi D^2}{4}-\frac{4\pi R_2^3}{3}\right]=-\beta\bar{U}\frac{\pi D^2}{4} \tag{17}$$

where, β represents the number of outlets in tube (β = 1 or 2). Solving for $\bar{U}$ yields

$$\bar{U}=\frac{16R_2^2}{\beta D^2}\frac{dR_2}{dt}=\frac{16R_1^2}{\beta D^2}\frac{dR_1}{dt} \tag{18}$$

Therefore, centerline and tube axial velocity is given by (using eq.(17) and eq.(14)),

$$V_{CL}=\alpha\frac{16R_2^2}{\beta D^2}\frac{dR_2}{dt} \tag{19}$$

Thus, final expression for V_z is given by:

$$V_z=\alpha\frac{16R_2^2}{\beta D^2}\frac{dR_2}{dt}\left[1-(\eta-1)\left(\frac{2r}{D}\right)^2\right] \tag{20}$$

In the above equations, the derivatives of R_2 and R_1 derivatives are interchangeable, by using mass conservation of shell as,

$$R_2^3-R_1^3=R_{20}^3-R_{10}^3=\delta V_o \tag{21}$$

Differentiating yields:

$$\frac{dR_2}{dt}=\frac{R_1^2}{R_2^2}\frac{dR_1}{dt} \tag{22}$$

$$\frac{d^2R_2}{dt^2}=\frac{R_1}{R_2^2}\left[R_1\frac{d^2R_1}{dt^2}+2\left(\frac{dR_1}{dt}\right)^2-2\frac{R_1^3}{R_2^3}\left(\frac{dR_1}{dt}\right)^2\right] \tag{23}$$

Eqs. (22) and (23) are frequently used in the subsequent derivation to convert first and second derivatives of R_2 to R_1.

Now the liquid pressure $P_L(R_2,t)$ can be obtained to get close for solution for eq.(10), integrating eq. (12) from shell interface to exit of the tube gives (along the centerline of tube):

$$\rho_F\int_{R_2(t)}^{L}\frac{\partial V_z}{\partial t}dz=\int_{R_2(t)}^{L}\left[-\frac{\partial p}{\partial z}+\mu_F\left[\frac{1}{r}\frac{\partial}{\partial r}\left(r\frac{\partial V_z}{\partial r}\right)\right]\right]dz \tag{24}$$

$$\int_{R_2(t)}^{L}\frac{\partial V_z}{\partial t}dz=k\left[R_1^2\frac{d^2R_1}{dt^2}+2R_1\left(\frac{dR_1}{dt}\right)^2\right](L-R_2) \tag{25}$$

$$\int_{R_2(t)}^{L}\mu_F\left[\frac{1}{r}\frac{\partial}{\partial r}\left(r\frac{\partial V_z}{\partial r}\right)\right]dz=\frac{16\mu_F S(1-\eta)(L-R_2)}{D^2} \tag{26}$$

$$\int_{R_2(t)}^{L}-\frac{\partial p}{\partial z}dz=P_L(R_2,t)-P_E \tag{27}$$

where,

$$k=\alpha\frac{16}{\beta D^2}\left[1-(\eta-1)\left(\frac{2r}{D}\right)^2\right] \quad and \quad S=\alpha\frac{16R_1^2}{\beta D^2}\frac{dR_1}{dt}, \tag{28}$$

and P_E is the liquid pressure at the exit of the tube. Therefore, final equation governing the liquid flow along the centerline of the tube (r=0) is given by :

$$P_L(R_2,t)=\alpha\frac{16\rho_L}{\beta D^2}\left[R_1^2\frac{d^2R_1}{dt^2}+2R_1\left(\frac{dR_1}{dt}\right)^2\right](L-R_2)-\frac{256\alpha\mu_F\rho_F R_1^2(1-\eta)(L-R_2)}{\beta D^4}\frac{dR_1}{dt}+P_E \tag{29}$$

The final model equation governing the dynamics of shelled micro-bubble or UCA in a tubular confinement can now be obtained by combining eq.(10) and eq.(24-29) which yields :

$$A\frac{d^2R_1}{dt^2}+B\left(\frac{dR_1}{dt}\right)^2+C\frac{dR1}{dt}+E=0 \tag{30}$$

where,

$$A=\rho_s(R_2-R_1)\frac{R_1}{R_2}+\frac{16\alpha\rho_F R_1^2(L-R_2)}{\beta D^2} \tag{31}$$

$$B=\rho_s\left[\frac{3}{2}+\frac{(R_1^3-4R_2^3)}{2R_2^3}\frac{R_1}{R_2}\right]+ \frac{32\alpha\rho_F R_1(L-R_2)}{\beta D^2} \tag{32}$$

$$C=4\mu_F\frac{R_1^2}{R_2^3}-4\mu_s R_1^2\left(\frac{1}{R_2^3}-\frac{1}{R_1^3}\right)+ \frac{256\alpha\rho_F\mu_F R_1^2(1-\eta)(L-R_2)}{\beta D^4} \tag{33}$$

$$E=\frac{2\sigma_1}{R_1}+\frac{2\sigma_2}{R_2}-P_o\left(\frac{R_o}{R_1}\right)^{3\gamma}-P_a+P_E \tag{34}$$

3. Results and Discussions

The proposed model, Eq.(30), is a second a order ordinary differential equation that fully describes the dynamics of shell micro-bubble or UCAs in a confined tube under acoustic field. In order to derive the dynamics of shelled micro-bubbles in other geometry confinement only appropriate mass conservation, like Eq.(17) needs to be written and rest of the derivation is trivial. The above model can be rigorously solved using fourth order Runge Kutta (Butcher 2008) method by utilization material properties and parameters involved in the experiments.

The proposed model was validated by numerically solving Eq. (30) against the experiment results of Zheng. et. al (Zheng, Dayton, Caskey, Zhao, Qin, and Ferrara 2007). Figure 2 shows the comparison of current model with the experiments. The parameters chosen to solve the model are the same acoustic and geometric parameters (acoustic frequency f=2.25 MHz, number of acoustic cycles N=20, at two peak negative pressures (PNP) of (a) PNP=175 KPa and (b) PNP=325 KPa, with initial bubble radius $R_{1o}=2\mu m$, $D=200\mu m$, $L=5cm$ as utilized in the experiments of Zheng. et. al (Zheng, Dayton, Caskey, Zhao, Qin, and Ferrara 2007). The values of fluid properties used in all calulation are $\rho_F=1000\ Kg/m^3$, $\rho_s=1200\ Kg/m^3$, $\mu_F=0.001\ Ns/m^2$, $\mu_s=0.05\ Ns/m^2$, $\sigma_1=0.072\ N/m$, $\sigma_2=0.052\ N/m$, and $P_o=101325\ N/m^2$, respectively.The temporal variation of the shelled micro-bubbles radius is also compared with the Church model (Church 1995) (with shell, using constitutive model of Newtonian fluid) and the Rayleigh Plesset (Brennen 1995) model (free bubble without shell) derived for the unconfined gas-bubble in the same figure. It can be clearly seen that for same acoustic and geometric conditions, Rayleigh Plesset model for free unconfined bubble oscillates highest, followed by Church model and the proposed model respectively. Results of the present model, when compared to the results of the Church and Rayleigh-Plesset models, show good agreement with the maximum experimental R/R_{1o} values.

The effects of geometric confinement are visible in Fig. 2. Apart from the amplitude of oscillation, the temporal dynamics response in terms of the oscillation frequency is also quite dissimilar for each investigated model. At lower PNP = 175 KPa (Fig. 2(a)), the bubble compression frequency is primarily dominated by a single frequency for the Rayleigh Plesset model, a subharmonic for the Church model, and several subharmonics are observed (small perturbations on primary curve) for the proposed model. For higher acoustic pressure, PNP = 325 KPa (Fig. 2(b)), Rayleigh Plesset and proposed model solution indicate a rise in per cycle amplitude after 3.8 μs and 2.2 μs, respectively. However, for the Church model, per cycle response in amplitude is fairly constant. In addition, for the proposed model case, the subharmonic frequency is significantly reduced compared to the low PNP case. It is potentially attributed to the diffusion of surface and parametric instabilities. The Rayleigh Plesset model has no shell encapsulation, and bubble response is in an infinite liquid pool. Thus, for this case, the fluid inertial forces dominate, and higher chances of inducing interfacial instabilities are possible. The Church model provides diffusive dampening due to the shell support at the interface. For the proposed model, apart from the shell diffusion, evolving fluid flow is restricted by the resistance created by the tube walls. It results in a more dampening and low dynamic response of the bubble during insonication. Thus, as anticipated, the geometric confinement not only dampens shelled micro-bubble oscillation but also affects the driving frequency.

From an applied perspective, an estimation of the resonant frequency of UCA in geometric confinement is important. For the case of free bubble, Oguz and Prosperetti (Oguz and Prosperetti 1998)

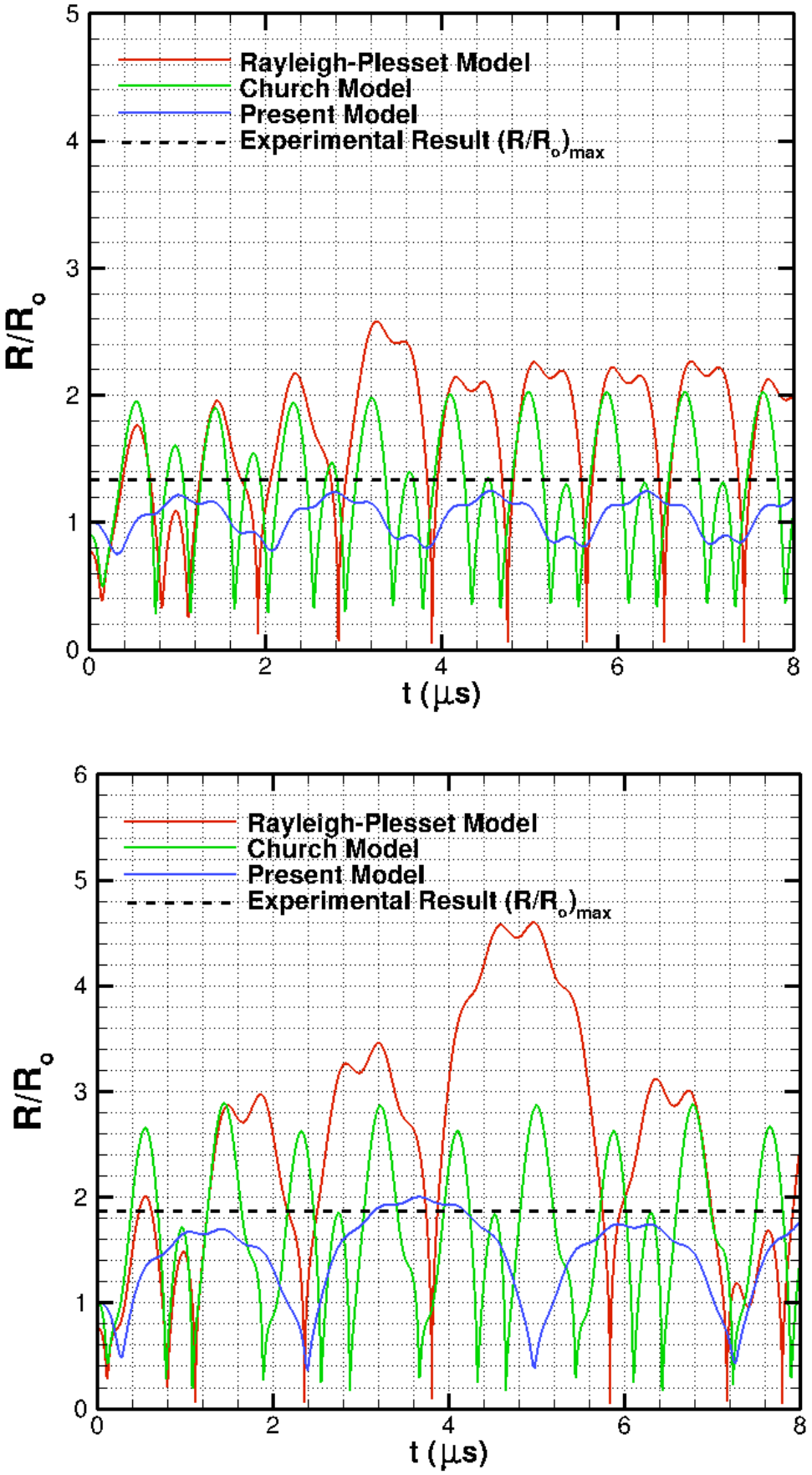

Fig. 2. Temporal Evolution of bubble radius as a function of time for R_{1o} = 2 micron at (a) PNP = 175 KPa (Left) and (b) PNP = 325 KPa (Right) for f=2.25 MHz and N=20

have theoretically computed the resonant frequency under varying configuration of geometric confinement in a rigid tube. However, for shelled microbubbles , there are no theoretical studies that can be used to estimate the resonant frequency in geometric confinement. The present model for the shelled micro-bubbled in geometric confinement, Eq.(30), is linearised in a manner similar to that in (Church 1995). This is done in order to obtained the linear harmonic equation which yield the expression for the resonant frequency of the shelled micro-bubble or UCA in circular cross-section confinement. The resonant frequency is quite useful from applied perspective especially in medical imaging and drug delivery, where bubble response to acoustic field is critical to avoid unreasonable outcomes. The proposed model is linearized and arranged in the form of a linear harmonic oscillator equation given by:

$$\ddot{X} + 2\xi_{tot}\dot{X} + \omega_r^2 X = 0 \tag{35}$$

with linearization achieved using $R_1 = R_{1_o}(1+X)$ and $R_2 = R_{2_o}(1+R_r X)$, where, $R_r = R_{1_o}^3/R_{2_o}^3$ and X is the perturbation amplitude as implemented by (Church 1995). After linearization, the resonant frequency for shell-micro-bubble is explicitly given as:

$$f_r = \frac{1}{2\pi R_{1o}} \sqrt{\frac{3P_o\gamma - \frac{2\sigma_1}{R_{1o}} - \frac{2\sigma_2}{R_{2o}}}{\rho_s \frac{(R_{2o}-R_{1o})}{R_{2o}} + \frac{16\alpha\rho_F R_{1o}(L-R_{2o})}{\beta D^2}}} \tag{36}$$

It is noteworthy, that resonant frequency for shelled micro-bubble with geometric confinement depends on geometric parameters of the confinement (L,D, β) and surrounding fluid properties (μ_F, ρ_F). However, for the case of free bubble (Church 1995) in unconfined space it is quite different which is given by :

$$f_{free} = \frac{1}{2\pi R_{1o}} \sqrt{\frac{3P_o\gamma}{\rho_F} + \frac{2(3\gamma-1)}{\rho_F R_{1o}}} \tag{37}$$

Figure 3(a) shows a comparison between the shelled micro-bubble resonant frequencies of the proposed model, with the free bubble case of Oguz and Prosperetti (Oguz and Prosperetti 1998) and that obtained by the use of the Boundary Element method (Oguz and Zeng 1995), in a tube of the same geometric dimensions. The resonant frequency is expected to be lower than free bubble case of (Oguz and Prosperetti 1998) and (Oguz and Zeng 1995), attributed to additional dampening created by shell material. The proposed model resonant frequency trend is similar to that of the free bubble in confinement with reduced resonant frequency as the initial micro-bubble size is increased. Furthermore, Fig. 3(b)-(c) shows the effect of variations in the geometric parameters (L, D) on the resonant frequency. The trends are similar to those unconfined free bubble case (Eq.(38)), i.e., the resonant frequency is inversely related to the initial bubble radius. For a small shelled micro-bubble, the resonant frequency is higher when compared to that for a large shelled micro-bubble as in the case of free bubble. For a shelled micro-bubble of fixed size, the resonant frequency is observed to vary proportionately to the diameter and inversely to square root of the tube length. Based on the self-similar nature of the behavior of the resonant frequency with geometric parameters, we utilize scaling arguments to collapse the resonant frequency data into a single curve. Fig. 3(d) shows the variation of the scaled frequency (scaled by $\sqrt{L}/D$) for various L/D ratios. For practitioners in this field, a curve fit in the form of a power law, is presented in Fig. 3(d) to estimate the resonant frequency of the shelled micro-bubbles or UCA in circular cross-section confinement.

Further, the linear dampening mechanism for the confined shell micro-bubble is also investigated. The viscous dampening coefficients are obtained, by linearising the proposed model according to Eq.(36), which yields :

$$\xi_{tot} = \frac{\xi_m}{\xi_c} \tag{38}$$

where,

$$\xi_m = 4\mu_F \frac{R_{1o}^3}{R_{2o}^3} - 4\mu_s R_{1o}^3 \left(\frac{1}{R_{2o}^3} - \frac{1}{R_{1o}^3}\right) + \frac{256\alpha\rho_F\mu_F R_{1o}^3(1-\eta)(L-R_{2o})}{\beta D^4}$$

$$\xi_c = \sqrt{\left[\rho_s(R_{2o}-R_{1o})\frac{R_{1o}^2}{R_{2o}} + \frac{16\alpha\rho_F R_{1o}^3(L-R_{2o})}{\beta D^2}\right]} \cdot \sqrt{\left[3P_o\gamma - \frac{2\sigma_1}{R_{1o}} - \frac{2\sigma_2}{R_{2o}}\right]}$$

It can be observed from above expression that for the constrained shell micro-bubble, viscous dampening is contributed by shell, liquid and geometric

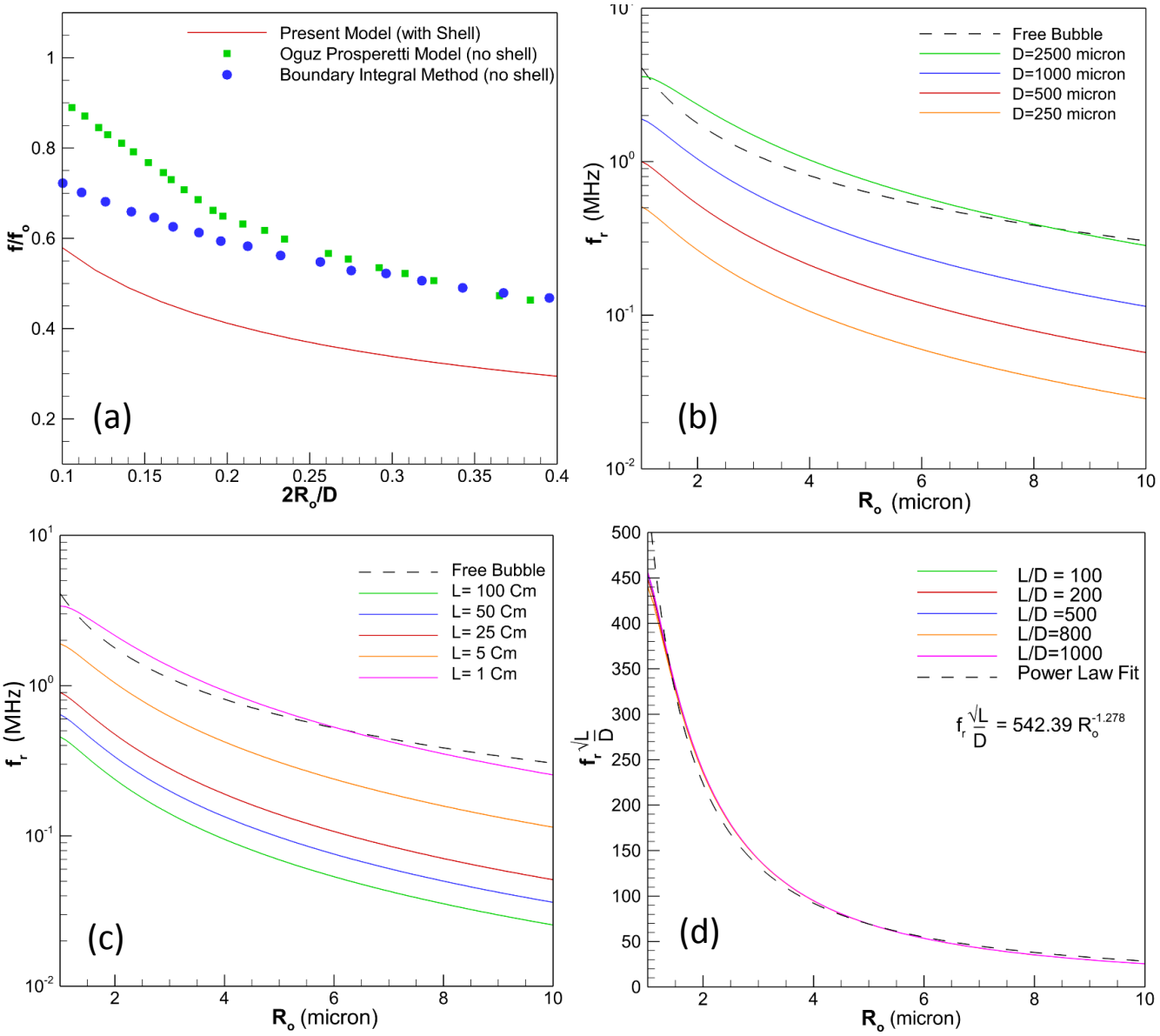

Fig. 3. Variation of linear resonant frequency with initial UCA radius (a) Comparisons with resonant frequency of free bubble (without shell) in a tube of L/D=5 with Oguz and Prosperetti theory and boundary element calculations. (b) Resonant frequency for various confinement diameter. (c) Resonant frequency for various confinement length. (d) Scaled resonant frequency for various L/D ratios.

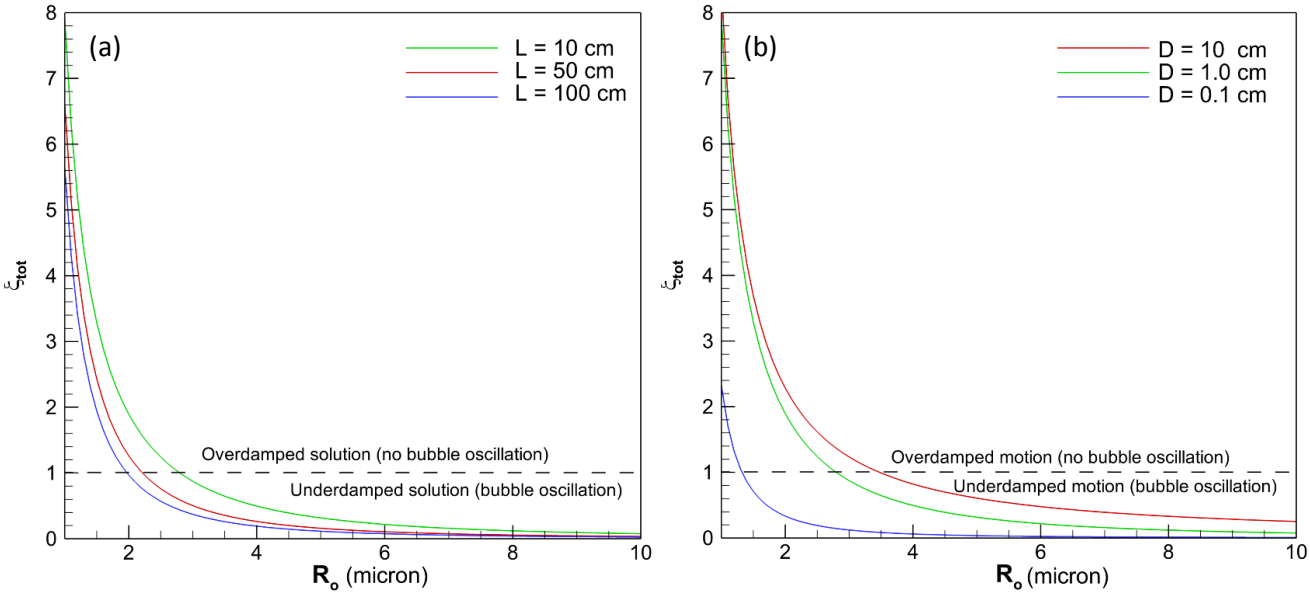

Fig. 4. Variation of linear viscous dampening coefficients with the initial shelled micro-bubble radius for various length (a) and diameter (b).

properties. Figure 4 shows the variation of viscous dampening coefficient as a function of initial micro-bubble size by varying the length, Fig. 4 (a), and diameter, Fig. 4 (b), of the tube, respectively. It can be seen that for a small R_{1o}, the total dissipation is higher for all D and L values. Further, an over-damped solution ($\xi_{tot} > 1$) exists in case of small shelled micro-bubble, suggesting no micro bubble oscillation, until triggered by oscillatory acoustic waves. In this phase the micro-bubble is expected to linearly follow the acoustic pressure pulse signature. In addition, as the diameter of the tube is increased the size of micro-bubble achieving over-damping state increases, Fig. 4(b). However, opposite trend is observed as the length of increased, Fig. 4(a). This may be attribute to the lower average fluid velocities in the tube when compared to the larger size shelled micro-bubbles. For the case when the bubble size shows underdamp solution by variation of L and D, it will be interesting to note that bubble response under acoustic field will be highly non-linear and proposed model such as described by Eq.(30) should be solved to clearly elucidate the dynamics of the shelled micro-bubble or UCA under geometric confinement.

4. Conclusions

A semi-analytical model for shelled micro-bubble in a geometric confinement, mimicking a rigid phantom vessel or tube is proposed. The model explicitly correlates all geometric, acoustic and fluid parameters to the dynamics of the shelled micro-bubble in confinement. Results of the model are compared with experimental data and reasonable comparison is observed. The natural linear resonant frequency and viscous damping coefficient are also derived. Resonant frequency is found to follow similar trend as in case of free bubble cases under confinement, but with more damping effects. A universal power fit law is also provided to predict the resonant frequency based on the dimensions of geometric confinement. Future studies will focus on extending the model to flexible confinement and incorporation of the base flow (pulsatile and uniform flow that exist in physiological conditions or applications where uniform flow prevails) to mimic real systems.

References

Atkisson, J. C. (2008). Models for acoustically driven bubbles in channels. *Phd Thesis, The University of Texas at Austin*.

Brennen, C. E. (1995). Cavitation and bubble dynamics. *Oxford University Press*.

Butcher, J. C. (2008). Numerical methods for ordinary differential equations. *Wiley; 2 edition*.

Caskey, C. F., D. E. Kruse, P. A. Dayton, and K. W. Ferrara (2005). On the oscillations of microbubbles in tubes with diameters as small as 12 microns. *IEEE, Ultrasonics Symposium 2*, 854–857.

Church, C. C. (1995). The effects of an elastic solid surface layer on the radial pulsations of gas bubbles. *Journal of the Acoustical Society of America 97*, 1510–1521.

Cosgrove, D. and C. Harvey (2009). Clinical uses of microbubbles in diagnosis and treatment. *Medical and Biological Engineering and Computing 47*, 813–826.

Dayton, P. A. and K. Ferrara (2002). Targeted imaging using ultrasound. *Journal of Magnetic Resonance Imaging 16*, 362–377.

Doinikov, A. A. and A. Bouakaz (2011). Review of shell models for contrast agent microbubbles. *IEEE Transactions on Ultrasonics, Ferroelectrics, and Frequency Control 58*, 981–993.

F.Caskey, C., D. E. Kruse, P. A. Dayton, T. Kitano, and K. W.Ferrara (2006). Microbubble oscillation in tubes with diameters of 12, 25, and 195 microns. *Applied Physics Letters 88*, 033902.

Garbin, V., D.Cojoc, E.Ferrari, E. D. Fabrizio, M. Overvelde, S. V. D. Meer, N. D. Jong, D.Lohse, and M. Versluis (2007). Changes in microbubble dynamics near a boundary revealed by combined optical micromanipulation and high-speed imaging. *Applied Physics Letter 90*, 114103.

Gueyffier, D., J. Li, A. Nadim, R. Scardovelli, and S. Zaleski (1999). Volume-of-fluid interface tracking with smoothed surface stress methods for three-dimensional flows. *Journal of Computational Physics 152*.

Humphrey, J. and S. Na (2002). Elastodynamics and arterial wall stress. *Annals Biomedical Engineering 30*.

Klibanov, A. L. (2006). Microbubble contrast agents: Targeted ultrasound imaging and ultrasound-assisted drug-delivery applications. *Investgative Radiology 41*, 354–362.

Leighton, T. G. (1994). The acoustic bubble. *Academic Press,San Diego,CA*, 67–196.

Lindner, J. R. (2004). Microbubbles in medical imaging: current applications and future directions. *Nature Reviews Drug Discoverys 3*.

Misra, J. and S. Singh (1983). A large deformation analysis for aortic walls under a physiological loading. *International Journal of Engineering Science 21*.

Oguz, H. N. and A. Prosperetti (1998). The natural frequency of oscillation of gas bubbles in tubes. *Journal of Acoustical Society of America 103*, 3301–3308.

Oguz, H. N. and J. Zeng (1995). Boundary integral simulations of bubble growth and detachment in a tube. *Boundary Element XVII, Computational mechanics publications, Madison,WI*, 645–652.

Pritchard, P. J. (2011). Fox and mcdonald's introduction to fluid mechanics. *Wiley; 8th Edition Binder Ready Version edition*.

P.Zhong, Y. F. Zhou, and S. L. Zhu (2001). Dynamics of bubble oscillation in constrained media and mechanisms of vessel rupture in SWL. *Ultrasound in Medicine and Biology 27*, 119–134.

Qamar, A., N. Hasan, and S. Sanghi (2006). New scheme for the computation of compressible flows. *AIAA Journal 44*.

Qamar, A., N. Hasan, and S. Sanghi (2010). A new spatial discretization strategy of the convective flux term for the hyperbolic conservation laws. *Engineering Applications of Computational Fluid Mechanics 4*.

Qamar, A., R. Samtaney, and J. L. Bull (2013). Dynamics of micro-bubble sonication inside a phantom vessel. *Applied Physics Letters 102*, 013702.

Qamar, A., Z. Z. Wong, J. B. Fowlkes, and J. L. Bull (2012). Evolution of acoustically vaporized microdroplets in gas embolotherapy. *Journal of Biomechanical Engineering 134*, 031010.

Ryu, K., S. K. Chung, and S. K. Cho (2010). Micropumping by an acoustically excited oscillating bubble for automated implantable microfluidic devices. *Journal of the Association for Laboratory Automation 15*, 163–171.

Sassaroli, E. and K. Hynynen (2004). Forced linear oscillations of microbubbles in blood capillaries. *Journal of Acoustical Society of America 115*, 3235–3243.

Sassaroli, E. and K. Hynynen (2006). On the impact of vessel size on the threshold of bubble collapse. *Applied Physics Letters 89*, 123901.

Unger, E. C., T. Matsunaga, T. McCreery, P. Schumann, R. Sweitzer, and R. Quigley (2002). Therapeutic applications of microbubbles. *European Journal of Radiology 42*, 160–168.

Ye, T. and J. L. Bull (2004). Direct numerical simulations of micro-bubble expansion in gas embolotherapy. *Journal of Biomechanical Engineering 126*, 745–759.

Zheng, H., P. A. Dayton, C. Caskey, S. Zhao, S. Qin, and K. W. Ferrara (2007). Ultrasound-driven microbubble oscillation and translation within small phantom vessels. *Ultrasound in Medicine and Biology 33*, 1978–1987.

Z.Z.Wong, O. Kripfgans, A. Qamar, J. Fowlkes, and J. L. Bull (2011). Bubble evolution in acoustic droplet vaporization at physiological temperature via ultra-high speed imaging. *Soft Matter 7*, 4009–4016.